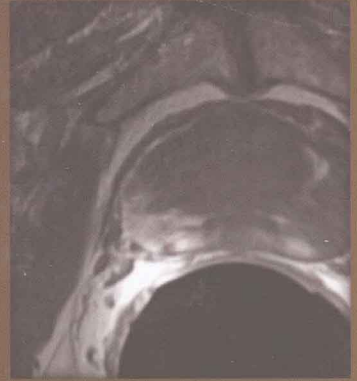
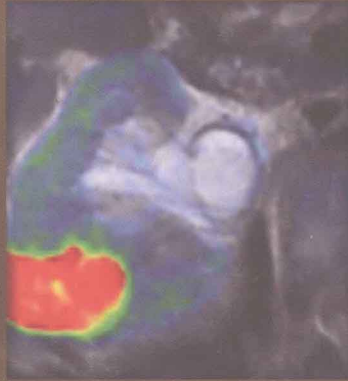




Practical Guide to

ABDOMINAL & PELVIC MRI

SECOND EDITION




John R. Leyendecker

Jeffrey J. Brown

Elmar M. Merkle



Wolters Kluwer | Lippincott Williams & Wilkins
Health



Practical Guide to Abdominal & Pelvic MRI

SECOND EDITION

John R. Leyendecker, MD

Associate Professor, Abdominal Imaging Section
Clinical Director, MRI
Department of Radiology
Wake Forest University School of Medicine
Winston-Salem, North Carolina

Jeffrey I. Brown, MD

Professor of Radiology
Co-Director, Body MRI
Director, Clinical Research Laboratory
Mallinckrodt Institute of Radiology
Washington University School of Medicine
St. Louis, Missouri

Elmar M. Merkle, MD

Professor of Radiology
Director of MR Imaging
Medical Director, Center for Advanced MR Development
Department of Radiology
Duke University Medical Center
Durham, North Carolina



Wolters Kluwer | Lippincott Williams & Wilkins

Health

Philadelphia • Baltimore • New York • London
Buenos Aires • Hong Kong • Sydney • Tokyo

Acquisitions Editor: Charles W. Mitchell
Product Manager: Ryan Shaw
Vendor Manager: Alicia Jackson
Senior Manufacturing Manager: Benjamin Rivera
Senior Marketing Manager: Angela Panetta
Design Coordinator: Stephen Druding
Compositor: Aptara, Inc.

© 2011 by LIPPINCOTT WILLIAMS & WILKINS, a WOLTERS KLUWER business

Two Commerce Square
2001 Market Street
Philadelphia, PA 19103

All rights reserved. This book is protected by copyright. No part of this book may be reproduced in any form by any means, including photocopying, or utilized by any information storage and retrieval system without written permission from the copyright owner, except for brief quotations embodied in critical articles and reviews. Materials appearing in this book prepared by individuals as part of their official duties as U.S. government employees are not covered by the above-mentioned copyright.

Printed in China

Library of Congress Cataloging-in-Publication Data

Leyendecker, John R.

Practical guide to abdominal and pelvic MRI / John R. Leyendecker,
Jeffrey J. Brown, Elmar M. Merkle. — 2nd ed.
p. ; cm.

Includes bibliographical references and index.

ISBN 978-1-60547-144-0 (hardback : alk. paper)

1. Abdomen—Magnetic resonance imaging—Handbooks, manuals, etc. 2.
Pelvis—Magnetic resonance imaging—Handbooks, manuals, etc. I. Brown,
Jeffrey J. II. Merkle, Elmar M. III. Title.

[DNLM: 1. Abdomen—pathology—Handbooks. 2. Magnetic Resonance
Imaging—methods—Handbooks. 3. Digestive System
Diseases—diagnosis—Handbooks. 4. Pelvis—pathology—Handbooks. WI 39
L683p 2011]

RC944.L394 2011

617.5'507548—dc22

2010025361

Care has been taken to confirm the accuracy of the information presented and to describe generally accepted practices. However, the authors, editors, and publisher are not responsible for errors or omissions or for any consequences from application of the information in this book and make no warranty, expressed or implied, with respect to the currency, completeness, or accuracy of the contents of the publication. Application of the information in a particular situation remains the professional responsibility of the practitioner.

The authors, editors, and publisher have exerted every effort to ensure that drug selection and dosage set forth in this text are in accordance with current recommendations and practice at the time of publication. However, in view of ongoing research, changes in government regulations, and the constant flow of information relating to drug therapy and drug reactions, the reader is urged to check the package insert for each drug for any change in indications and dosage and for added warnings and precautions. This is particularly important when the recommended agent is a new or infrequently employed drug.

Some drugs and medical devices presented in the publication have Food and Drug Administration (FDA) clearance for limited use in restricted research settings. It is the responsibility of the health care provider to ascertain the FDA status of each drug or device planned for use in their clinical practice.

To purchase additional copies of this book, call our customer service department at (800) 638-3030 or fax orders to (301) 223-2320. International customers should call (301) 223-2300.

Visit Lippincott Williams & Wilkins on the Internet: at LWW.com. Lippincott Williams & Wilkins customer service representatives are available from 8:30 am to 6 pm, EST.

10 9 8 7 6 5 4 3 2 1

To Mary, Michael, and Bridget for their love and support.

JRL

For my wife, Ann, and my children, Preston, Nathan, and Kalli.

JJB

To my wife Christina, and my daughters Paula and Anna.

EMM

Preface

When we wrote the first edition of *Practical Guide to Abdominal and Pelvic MRI*, we sought to create a readable text that addressed the gap that existed at the time between detailed and comprehensive reference books about abdominal magnetic resonance imaging (MRI) and more focused writings such as review articles, technical manuals, and organ-centered texts. Ours was a book targeting the practicing radiologist who wanted to produce, and accurately interpret, excellent quality abdominal MRI examinations in the setting of a busy practice with little or no background in MR-related physics. To keep the text short, we focused on common clinical scenarios and limited explanations to convey only the most relevant information.

From inception through completion of the second edition, we have once again tried to put ourselves in the place of a practicing radiologist confronted with the challenge of sifting through the unrelenting barrage of new MR sequences, acronyms, and clinical applications inherent to the field of abdominal MRI. The challenge in producing this edition has been to maintain the spirit of the first edition while keeping pace with this expanding field. While the growing sophistication of abdominal MR practitioners demanded that we update and expand the discussions of physical principles, we sought to maintain the brevity and practical focus of the first edition. Therefore, much of the increased length of this new edition results from inclusion of new, state-of-the-art MR images reflecting enhancements in MR system hardware, pulse-sequences, and coil design. We have also expanded and indexed the atlas of MRI abnormalities to reflect the growing variety of clinical indications for abdominal MRI.

With this second edition comes also a new coauthor, Elmar Merkle. Dr. Merkle brings with him years of experience with advanced MR imaging techniques, a clinically relevant focus, and a fresh educational perspective. His contributions to the second edition have been as substantial and insightful as they have been welcome. His expertise has allowed the addition of a chapter on new techniques in abdominal and pelvic MRI that explains the challenges of imaging the abdomen at 3 Tesla, diffusion-weighted imaging, and the potential uses of MR spectroscopy. Through our collaboration with Dr. Merkle, we have greatly increased the number of high-quality, clinically relevant images, and his experience with a variety of vendor platforms and new technologies will no doubt broaden the appeal of this new edition.

We believe this book contains a distillate of much of the clinically relevant information currently available about abdominal and pelvic MRI. However, we acknowledge that gaps will develop in this information as the field advances. Therefore, we consider our book a first step in understanding and implementing abdominal MRI techniques in clinical practice and encourage our readers to continually build on this knowledge as the field evolves. We think this book will appeal to radiology trainees as well as practicing radiologists, and we sincerely hope that residents will find sufficient inspiration in its pages to pursue a career in this exciting field.

John R. Leyendecker, MD
Jeffrey J. Brown, MD
Elmar M. Merkle, MD



Acknowledgments

Many thanks to the people at Wolters Kluwer Health/Lippincott Williams & Wilkins and, in particular, Ryan Shaw, who helped make this edition of our textbook a reality. Thanks to Elmar Merkle and Jeffrey Brown for their valuable suggestions and contributions, without which this book could not have been completed. Finally, thanks to my many friends and colleagues in the abdominal MRI community who still see value in academic pursuits and whose teachings and inspiration are reflected in this book.

John R. Leyendecker, MD

I thank my coauthors, John Leyendecker and Elmar Merkle, whose intelligence, clarity, and vision were the driving forces behind this book.

Jeffrey J. Brown, MD

First, I thank John Leyendecker and Jeffrey Brown for giving me the opportunity to become a coeditor. This provided me a unique platform to share my point of view about body and pelvic MRI with the radiology community. I also acknowledge the help of Brian J. Soher, PhD; he solely contributed the section about MR spectroscopy in a very “readable” fashion. Thorsten A. Bley, MD, contributed tremendously to the MR angiography chapter, and I am most grateful for his excellent work. Furthermore, I acknowledge my partners Mustafa S.R. Bashir, MD, and Rajan T. Gupta, MD, for proofreading the entire book. Finally, I thank my wife, Christina, and my daughters, Paula and Anna, for tolerating my many weekends away from home.

Elmar M. Merkle, MD



Contributors

Thorsten A. Bley, MD

Assistant Professor of Radiology
Department of Radiology
University Medical Center Hamburg-Eppendorf
Hamburg, Germany
Chapter 2.1, Magnetic Resonance Angiography

Markus Lämmle, MD

Assistant Professor of Radiology
Director, Magnetic Resonance Imaging
Diagnostic Imaging Service
St. Louis VA Medical Center—John Cochran Division
Saint Louis, Missouri
Chapter 2.4, Magnetic Resonance Imaging of the
Gastrointestinal Tract

Pratish Shah, MD

Research Assistant
Wake Forest University School of Medicine
Winston-Salem, North Carolina
Chapter 3.3, Atlas of MRI Abnormalities

Brian J. Soher, PhD

Assistant Professor, Radiology
Center for Advanced MR Development
Duke University Medical Center
Durham, North Carolina
Chapter 1.5, New Techniques in Abdominal
and Pelvic MR Imaging

Contents

| | |
|------------------------|------------|
| <i>Preface</i> | <i>v</i> |
| <i>Acknowledgments</i> | <i>vi</i> |
| <i>Contributors</i> | <i>vii</i> |

■ Section 1: Imaging the Abdomen and Pelvis

| | | |
|-------|--|----|
| ■ 1.1 | Basic Magnetic Resonance Imaging Principles for the Abdomen and Pelvis | 2 |
| ■ 1.2 | Scan Optimization: The Art of Compromise | 22 |
| ■ 1.3 | Modifying Sequence Parameters | 37 |
| ■ 1.4 | Using Magnetic Resonance Contrast Agents in the Abdomen and Pelvis | 41 |
| ■ 1.5 | New Techniques in Abdominal and Pelvic MR Imaging | 63 |
| ■ 1.6 | Abdominal and Pelvic Protocol Basics | 82 |

■ Section 2: Introduction to Specific Abdominal and Pelvic Magnetic Resonance Imaging Techniques

| | | |
|-------|--|-----|
| ■ 2.1 | Magnetic Resonance Angiography | 106 |
| ■ 2.2 | Magnetic Resonance Cholangiopancreatography | 130 |
| ■ 2.3 | Magnetic Resonance Urography | 144 |
| ■ 2.4 | Magnetic Resonance Imaging of the Gastrointestinal Tract | 158 |
| ■ 2.5 | Maternal MRI during and after Pregnancy | 171 |

■ Section 3: Interpretation of Abdominal and Pelvic Magnetic Resonance Imaging

| | | |
|-------|--|-----|
| ■ 3.1 | Approach to Interpreting Abdominal and Pelvic MRI Examinations | 186 |
| ■ 3.2 | Atlas of Abdominal and Pelvic Magnetic Resonance Imaging Anatomy | 194 |
| ■ 3.3 | Atlas of MRI Abnormalities | 209 |
| ■ 3.4 | Differential Diagnoses for Abdominal and Pelvic Magnetic Resonance Imaging | 326 |

■ Section 4: Additional Useful Information

| | | |
|-------|---|-----|
| ■ 4.1 | Magnetic Resonance Imaging Acronyms and Abbreviations | 386 |
| ■ 4.2 | Glossary of Magnetic Resonance Imaging Terms | 392 |

| | |
|--------------|------------|
| <i>Index</i> | <i>397</i> |
|--------------|------------|



Section 1

Imaging the Abdomen and Pelvis



Section 1.1

Basic Magnetic Resonance Imaging Principles for the Abdomen and Pelvis

A basic understanding of a limited number of physical principles is essential to performing and interpreting abdominal and pelvic magnetic resonance imaging (MRI) examinations. However, it is not necessary, or even advisable, for most radiologists to understand MRI physics at the quantum level to perform high-quality clinical MRI studies. Few of us fully understand Einstein's description of gravity in his general theory of relativity, but none of us would willingly vacate an airplane at 15,000 feet without a parachute. In other words, a full understanding of the physics or mathematics of gravity is unnecessary to predict the behavior of an object within a gravitational field. Similarly, an in-depth understanding of MR physics remains a luxury for most of us. Therefore, this discussion focuses on the principles that are most relevant to the practical needs of radiologists.

Most of the discussions of MR physics in this text are based on Newtonian approximations. An understanding of the behavior of individual protons requires knowledge of quantum mechanics. However, because MRI measures the signal of large populations of protons rather than individual protons, Newtonian approximations are sufficient to predict behavior, which is really what interests clinical imagers. Attempts to explain all MRI phenomena using only Newtonian models may eventually result in frustration and confusion. Therefore, our simplistic explanations should be viewed not so much as statements of ultimate truth but rather as practical mnemonic devices beneficial to the clinical application of MR. The reader can take comfort in knowing that even Albert Einstein had trouble accepting many of the tenets of quantum physics despite his own contributions to the field.



HOW DOES MRI WORK?

Most MRI systems are built around a superconducting magnet. In the simplest sense, a superconducting magnet consists of highly conductive wire coiled around the bore of the magnet and encased in a cryogen such as liquid helium. By cooling the wire to very low temperatures (typically <10 Kelvin), resistance is nearly eliminated, creating a **superconductor**, in which an electrical current established in the wire will continue unabated for a long time.

An electrical current moving through a coiled wire is associated with a magnetic field, which in the case of a typical superconducting MRI magnet has field lines oriented along the longitudinal axis of the magnet bore. These field lines represent the main magnetic field typically referred to

as "**B₀**." Once a patient is placed in the scanner, some of the patient's protons align with B₀. Because protons can be thought of as spinning charged particles, they are associated with a small magnetic field referred to as a "magnetic dipole moment". This magnetic field may be represented as a vector along the axis of the spinning proton. Normally, the magnetic field vectors of all the body's protons are randomly aligned. When placed in a strong external magnetic field (such as an MRI scanner), these vectors align parallel or antiparallel to the main magnetic field.* Because slightly more proton vectors align in the parallel direction than in the antiparallel direction, a net magnetization vector results, representing the sum of the individual magnetization vectors of the protons. This net magnetization vector (often denoted as M₀) is referred to as **longitudinal magnetization**. The magnitude of M₀ is proportional to the strength of the external field B₀ and also determines how much signal can ultimately be obtained in clinical MRI. This helps to explain much of the interest in higher field strength MR scanners.

The individual magnetic field vectors of protons placed in the MRI scanner do not align perfectly with the external field. Instead, they precess about the external magnetic field vector much like the earth precesses in space or a top precesses under the influence of gravity (Fig. 1.1.1). In addition, the individual protons precess out-of-phase with one another much like a random assortment of spinning tops would be tilted slightly in different directions at any moment in time. Protons existing in a similar chemical environment and uniform external magnetic field precess at the same frequency according to the **Larmor equation**:

$$\text{Resonant frequency (MHz)} = (42.6 \text{ MHz/tesla})(\text{magnetic field strength [in tesla]})$$

This equation expresses mathematically that the precessional frequency of protons is directly proportional to the strength of the external magnetic field. In other words, hydrogen protons precess slower at 0.5 T than they do at 1.5 Tesla (1.5T). This has important implications for how signal from protons is localized in space

*The description of protons aligned parallel and antiparallel to the main magnetic field serves as a graphic representation of protons in low- and high-energy states, respectively. The energy differential between low- and high-energy states is proportional to the external magnetic field strength.

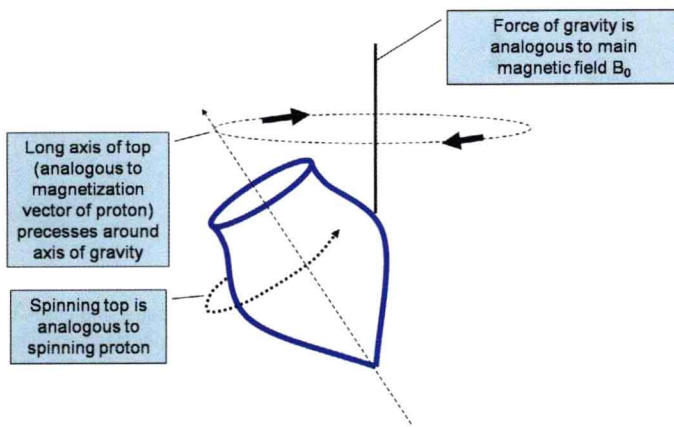


FIG. 1.1.1. Concept of precession. In the classical model, protons can be thought of as spinning charged particles associated with small magnetization vectors. These vectors precess about the main magnetic field, B_0 , like tops precessing around a gravitational field. When brought into phase, the sum of these small magnetization vectors form the net magnetization vector M_0 , which also precesses about B_0 .

and for techniques such as chemically selective fat suppression. The value 42.6 MHz/tesla is the gyromagnetic ratio for a hydrogen nucleus (proton) in a water molecule, the source of most clinically relevant MRI signal.

To generate signal from protons placed within a magnet, two things must be accomplished. First, the protons must be made to precess in-phase (i.e., their magnetic field vectors should point in the same direction). Second, the net magnetic field vector must be tipped from the longitudinal axis (aligned with the external magnetic field) into the transverse plane (aligned perpendicular to the external magnetic field). This latter condition results from the need to create an oscillating magnetic field in the patient that generates a current (the echo) in the receiver coil. In other words, just as current moving in the coiled wire of the magnet is associated with a magnetic field, a rotating magnetic field in the patient can induce a current in the coiled wire of the receiver coil. These two conditions (creation of **transverse magnetization** and **phase coherence**) are accomplished with the application of a radiofrequency (RF) pulse at the resonant frequency of hydrogen protons.

The application of the RF pulse (which can be thought of as an oscillating magnetic field) causes the longitudinal magnetization vector to spiral down into the transverse plane so that it can be measured. This initial RF pulse is commonly referred to as an **excitation pulse** or alpha (α) pulse. The degree to which longitudinal magnetization is converted into transverse magnetization depends on the amplitude and duration of the RF pulse. The angle between the original longitudinal magnetization and the new net magnetization vector created by the RF pulse is referred to as the **flip angle**.

The relationship between the main magnetic field (B_0), the net magnetization vector of the patient, and the RF pulse is somewhat analogous to a game of tetherball. Gravity can be thought of as the main magnetic field, the tether from which the ball hangs can be thought of as the net magnetization vector of the patient, and a hand

hitting the ball can be thought of as the RF pulse. If the hand hits the ball repeatedly at the same rate as the orbital frequency of the ball around the pole, the ball will eventually spiral into a plane perpendicular to the direction of force of gravity (analogous to the transverse plane). Of course, this analogy assumes that the string does not wrap around the pole and shorten with each revolution. Expanding the analogy, a group of hands hitting a group of balls with the same force, at the same time, and at the same location will cause the balls to become “in-phase” as they revolve around their respective poles. This is analogous to multiple protons precessing in-phase in response to the RF excitation pulse.

The transverse magnetization created within the patient can be thought of as an oscillating magnetic field oriented perpendicular to B_0 . The **receiver coil** (which functions as an antenna) is made of a conductive metal alloy. When an electrical conductor exists in the presence of a changing magnetic field, a current is induced (according to **Faraday’s law** of induction). It is in this manner that the MR signal is “collected.” In other words, the changing magnetic field induced in the patient by the excitation pulse induces a current in the receiver coil.

Various other explanations for generation of the MR signal have been described that are equally valid (and in many cases, equally fallible if taken too far). Our advice is to find a means of conceptualizing these complex phenomena with which you are comfortable, acknowledging that the purpose of all such models is to facilitate the clinical application of magnetic resonance, not to imbue the user with profound insights into the mysteries of the subatomic universe.



T1 AND T2

Most abdominal and pelvic MR images fall into one of two categories: **T1-weighted (T1W)** or **T2-weighted (T2W)**. These terms describe the creation of image contrast based on the T1 and T2 **relaxation times** of tissues. Differences in T1 relaxation times between tissues determine the image contrast in a T1W image, and differences in T2 relaxation times between tissues determine the image contrast in a T2W image. MR images are referred to as *weighted*, because no image represents differences only in T1 or T2 relaxation times. There is always some T2 contrast in a T1W image and some T1 contrast in a T2W image. Figure 1.1.2 illustrates the differences between these two types of images. One class of pulse sequences, referred to as “balanced steady-state free precession,” is considered to have contrast weighting based on the ratio of T2 to T1 (T2/T1 weighting). Balanced steady-state free precession sequences can be recognized by the very high signal intensity of both extravascular fluid and intravascular blood with minimal flow-related artifact.

The source of the signal measured by MRI is hydrogen nuclei (i.e., protons). When these protons are exposed to an RF pulse, phase coherence is created (the protons precess in-phase), and transverse magnetization is created (the net magnetization vector spirals into the transverse plane). Once the RF pulse is shut off, the protons begin to realign with the external magnetic field (B_0). As this

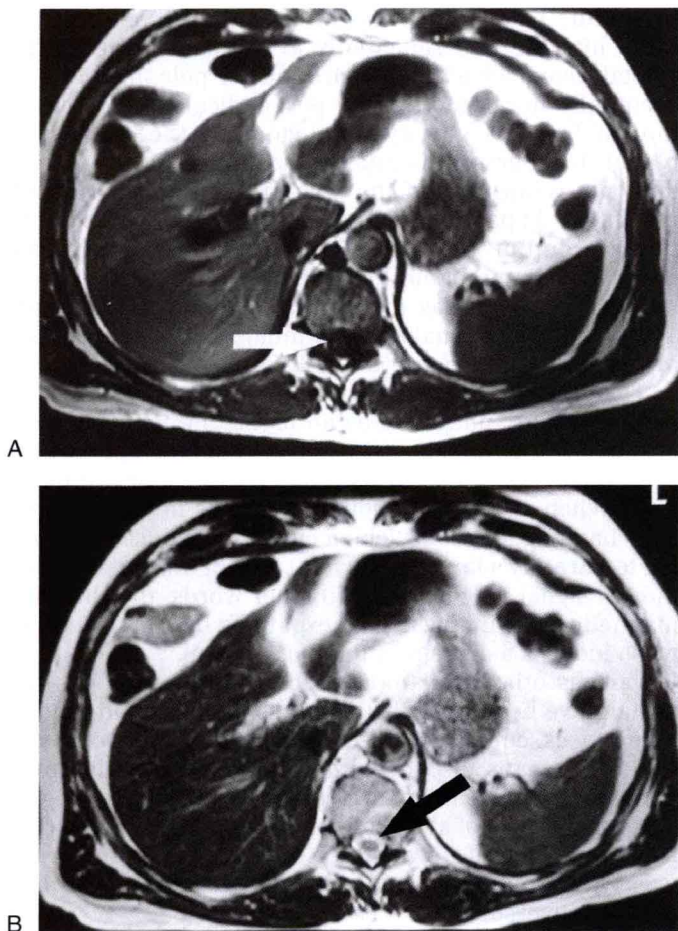


FIG. 1.1.2. T1W image versus T2W image. **A:** Axial T1W spin echo image. Bright fat and dark fluids (cerebrospinal fluid [CSF]) (arrow) are characteristic of T1W images. The signal intensity of liver is normally slightly greater than that of spleen. **B:** Axial T2W fast spin echo image. Bright fluid (CSF) (arrow) is characteristic of T2W images. Fat is also bright on fast spin echo images. Signal intensity of spleen is normally slightly greater than that of liver, a difference that is considerably more apparent on fat-suppressed images.

occurs, the net longitudinal magnetization vector regrows in a logarithmic fashion. The time it takes for approximately two thirds (63%) of the original longitudinal magnetization to regrow is referred to as the **T1 relaxation time** (longitudinal relaxation time) (Fig. 1.1.3).

While T1 relaxation (regrowth of longitudinal magnetization) is occurring, there is also a decay of transverse magnetization. Although regrowth of longitudinal magnetization and loss of transverse magnetization occur simultaneously, we encourage readers to *think of these as separate processes* occurring at different rates in most tissues. Transverse magnetization decay usually occurs much faster than regrowth of longitudinal magnetization. The loss of transverse magnetization (an exponential decay function) results from both an energy exchange between protons (referred to as “spin-spin interaction”) and heterogeneity in the magnetic field strength caused by imperfections in the scanner itself or the material (e.g., metal, air, tissue) placed within the scanner. The

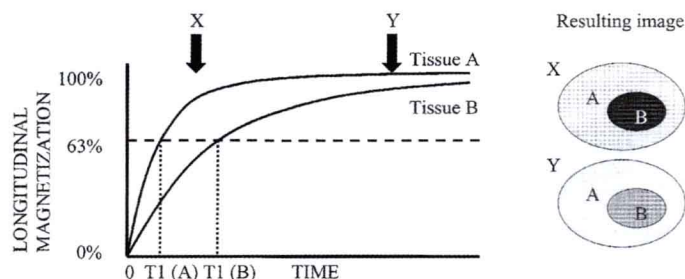


FIG. 1.1.3. T1 relaxation and T1 contrast. At time = 0, tissue A and tissue B are subjected to a 90-degree RF pulse, eliminating longitudinal magnetization. Tissue A recovers its longitudinal magnetization more quickly than does tissue B and, therefore, has shorter T1 (when it recovers approximately 63% of its initial longitudinal magnetization). At time X (arrow X), there is a relatively large difference in longitudinal magnetization between tissue A and tissue B. Therefore, an image based on this difference (upper oval to right of graph) would have excellent T1 contrast. An image based on the difference in longitudinal magnetization at time Y (arrow Y) would have considerably less image contrast (lower oval to right of graph).

loss of transverse magnetization resulting from the interaction between hydrogen nuclei (spin-spin interactions) is an irreversible process known as **T2 decay**. The time it takes for transverse magnetization to decay to approximately one third (37%) of its maximum value as a result of this irreversible process is referred to as the **T2 relaxation time** (Fig. 1.1.4).

The magnet's main magnetic field, B_0 , is relatively homogeneous (within a few parts per million) when the bore is empty. However, once a patient is placed in the magnet bore, the field experienced by the patient is less homogeneous, largely due to different magnetic susceptibilities of the various tissues. The loss of transverse magnetization resulting from these static variations in local magnetic field strength is a reversible process that occurs very rapidly. This decay occurs because protons precess

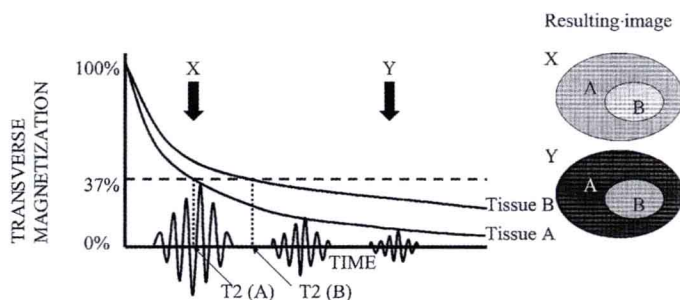


FIG. 1.1.4. T2 relaxation and T2 contrast. At time = 0, tissue A and tissue B are subjected to a 90-degree RF pulse, creating transverse magnetization. This excitation pulse is followed by three 180-degree refocusing pulses that result in three echoes (wavy lines). Echoes only for tissue A are shown. The T2 relaxation curve follows echo peaks. Note that tissue A loses its transverse magnetization more rapidly than does tissue B and, therefore, has a shorter T2 (when it decays to approximately 37% of its initial value). At time X (arrow X), there is a relatively small difference in transverse magnetization between tissue A and tissue B. Therefore, an image based on this difference (upper oval to right of graph) would have poor T2 contrast. An image based on the difference in transverse magnetization at time Y (arrow Y) would have considerably more image contrast (lower oval to right of graph).

Creation of a Spin Echo

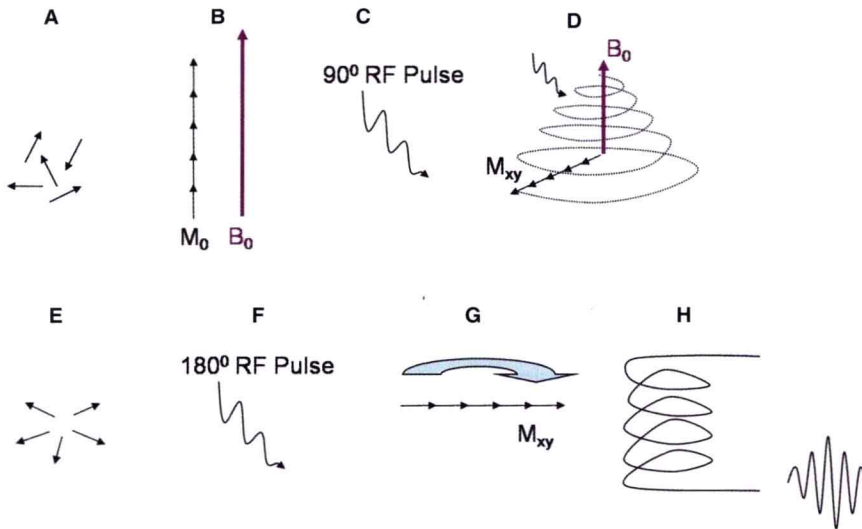


FIG. 1.1.5. The steps involved in the creation of a spin echo. **A:** Before placing a patient in the magnet bore, the magnetization vectors of hydrogen protons are randomly aligned and are not associated with any net magnetization vector. **B:** Once the patient is placed in the magnet bore, the protons align with B_0 such that net magnetization is created through the sum of the individual vectors (some protons align antiparallel to B_0 , but we have simplified things here). **C:** A radiofrequency pulse (oscillating magnetic field) is applied to the protons at their precessional frequency. This creates phase coherence (protons precess in-phase) such that M_0 now precesses around B_0 . **D:** During continued application of the RF pulse, M_0 spirals into the transverse plane (now designated as M_{xy}). **E:** Phase coherence established during application of the RF pulse is rapidly lost once the RF pulse is turned off. **F:** A 180-degree RF pulse is applied, reversing phase dispersion induced by local magnetic field inhomogeneities and bringing the protons back into phase. **G:** With reestablishment of phase coherence, a net magnetization vector M_{xy} is reestablished. **H:** M_{xy} continues to rotate in the transverse plane about B_0 . This rotating magnetic field induces a current (the echo) in a receiver coil.

at slightly different rates when exposed to different local magnetic field strengths (according to the Larmor equation). Protons precessing at different rates rapidly lose phase coherence, which, in turn, reduces the magnitude of the net magnetization vector in the transverse plane. This more rapid loss (decay) of transverse magnetization (along with T2 decay) is referred to as **free induction decay**, characterized by the term **T2***. T2* is always shorter than T2, and T2 cannot be longer than T1. The magnetic field heterogeneities responsible for T2* decay can create geometric distortion in the final image.

Different tissues in the body have different intrinsic T1 and T2 values. For example, water has relatively long T1 and T2 values, whereas fat has T1 and T2 values that are considerably shorter. A tissue with a short T1 recovers longitudinal magnetization faster than a tissue with a long T1 and therefore appears brighter on a sequence designed to bring out the differences in T1 relaxation (a T1W scan). A tissue with a short T2 loses transverse magnetization quicker than a tissue with a long T2 and therefore appears darker on a sequence designed to bring out differences in T2 relaxation (a T2W scan). These differences in T1 and T2 values give rise to most of the tissue contrast seen in abdominal and pelvic MRI.



SPIN ECHO VERSUS GRADIENT ECHO

One of the major components of the MRI pulse sequence is the RF excitation pulse, which is used to convert net longitudinal magnetization into net transverse magnetization. For a typical spin echo sequence, this pulse is 90 degrees, which means that essentially all of the initial longitudinal magnetization is converted into transverse magnetization. However, the initial net transverse magnetization decays too rapidly to be of much use in generating an image. This is because the transverse magnetization vectors of the individual protons rapidly lose their phase coherence (they become out-of-phase with each

other), resulting in loss of net magnetization. This loss of phase coherence results from several sources, including the T2* effects discussed earlier as well as the magnetic gradients used for spatial localization. To obtain a more useful signal from which an MR image can be made, either RF refocusing or gradient refocusing is used to bring the individual transverse magnetization vectors back into phase.

The **spin echo** family of pulse sequences makes use of a 180-degree RF pulse to bring the protons back into phase to create the echo, a process known as “RF refocusing.” The effect of the 180-degree pulse is to flip the individual transverse magnetization vectors so that the more rapidly precessing protons catch up with the slower protons, much like runners of different speeds realigning after their direction is reversed. The process of creating a spin echo is illustrated in Figure 1.1.5. A refocusing pulse of less than 180 degrees also creates an echo, but a 90- and 180-degree RF pulse combination gives the maximum signal.

Because a 180-degree pulse results in the strongest echo, one might think that it is always the optimal RF refocusing pulse. For a simple spin echo sequence, this is generally true. However, a 180-degree RF pulse is also associated with higher-energy deposition in the patient (manifested as tissue heating) than is a pulse with a lower flip angle, because the higher flip angle requires increased amplitude or duration of the RF pulse.* The use of a large number of 180-degree refocusing pulses (as may occur with fast spin echo [FSE] or turbo spin echo [TSE] imaging) can result in unacceptably high levels of energy deposition in the body, particularly if the RF

*The amount of energy deposited in a patient as a result of RF pulses is referred to as the *specific absorption rate* (SAR). Increases in flip angle, number and frequency of RF pulses, and main magnetic field strength all contribute to increases in SAR.

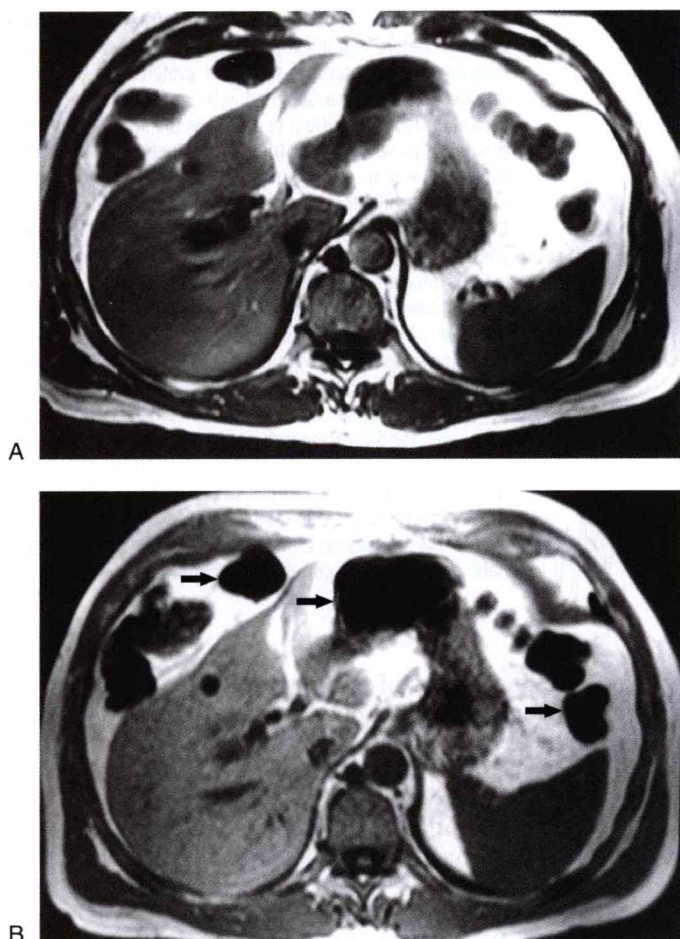


FIG. 1.1.6. Spin echo versus gradient echo. **A:** This axial spin echo T1W image is the same as in Figure 1.1.2A. Acquisition time was approximately 2 minutes for the complete liver. Respiratory motion artifact was reduced by placement of a saturation band over anterior abdominal fat. **B:** Axial gradient echo T1W image of the same patient. The entire liver was imaged in less than 30 seconds during a single breath-hold. The image has increased noise and more susceptibility artifact around the bowel (arrows) than does the spin echo image.

pulses are spaced closely together. One way to prevent tissue heating and conform to Food and Drug Administration regulations is to reduce the refocusing pulses to less than 180 degrees.

In contrast to spin echo sequences, **gradient echo** sequences use only gradient reversals to bring the protons back into phase to create the echo. As a result, there are no 180-degree refocusing pulses in gradient echo imaging. **Gradients** are linear variations in magnetic

field strength that are applied at specific times during a pulse sequence. A gradient applied along one axis of the body causes the protons along that gradient to precess at different frequencies according to the Larmor equation. Protons exposed to higher field strengths precess at higher frequencies than do protons exposed to lower field strengths. The result of these different precessional frequencies is that the protons begin to dephase. By reversing this gradient, the protons can be made to rephase (gradient refocusing). One important difference between gradient refocusing and RF refocusing is that the former technique corrects only for dephasing induced by the initial gradient, whereas the latter technique also corrects for the effects of local magnetic field heterogeneities. Therefore, gradient echo pulse sequences are more susceptible to artifacts created by substances that alter the local magnetic environment of the protons, such as metal or air. Gradient echo sequences are preferred for the detection of tissue iron deposition (e.g., hemochromatosis), and spin echo sequences are preferred in the setting of implanted metallic prostheses (to reduce artifacts). The initial RF excitation pulse is often less than 90 degrees for a gradient echo sequence, but any flip angle up to 90 degrees may be used. Spin echo sequences also correct for the dephasing induced by imaging gradients. Examples of spin echo and gradient echo images are shown in Figure 1.1.6.

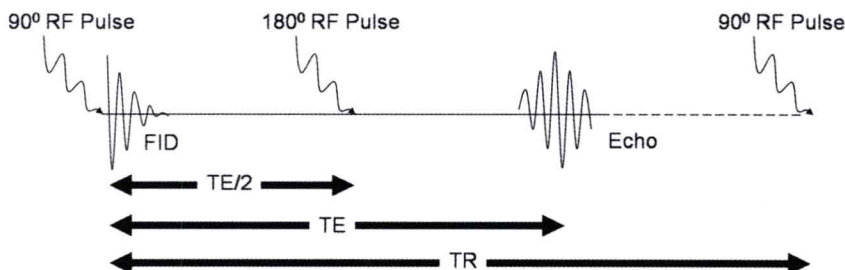
One more word about gradient echo sequences is appropriate here. One often hears the term “spoiled” in association with gradient echo imaging. The term “spoiling” refers to the elimination of residual transverse magnetization between successive excitations. This is generally accomplished through the application of a strong magnetic gradient to induce dephasing in the transverse plane. Most abdominal gradient echo MR sequences are spoiled, because persistent residual transverse magnetization can have undesirable effects on the image. Steady-state free precession sequences (commonly used to image the heart) are unspoiled gradient echo sequences.



REPETITION TIME AND ECHO TIME

T1 and T2 are physical properties inherent to the tissues being imaged, whereas the **repetition time (TR)** and **echo time (TE)** are imaging parameters that can be modified by the operator of the MR system (Fig. 1.1.7). To spatially encode MRI data, the tissue protons must undergo a series of steps referred to as **phase encoding**. For most MRI sequences, the initial RF excitation pulse and the refocusing pulse (in the case of spin echo) or

FIG. 1.1.7. Repetition time (TR) and echo time (TE) for spin echo sequence. TR represents elapsed time between successive 90-degree excitations. TE represents the time delay from the 90-degree excitation to the center of the echo. Note that the 180-degree refocusing pulse occurs at time = $\frac{1}{2}$ TE. FID, free induction decay.



Creation of equilibrium through the application of repeated RF pulses

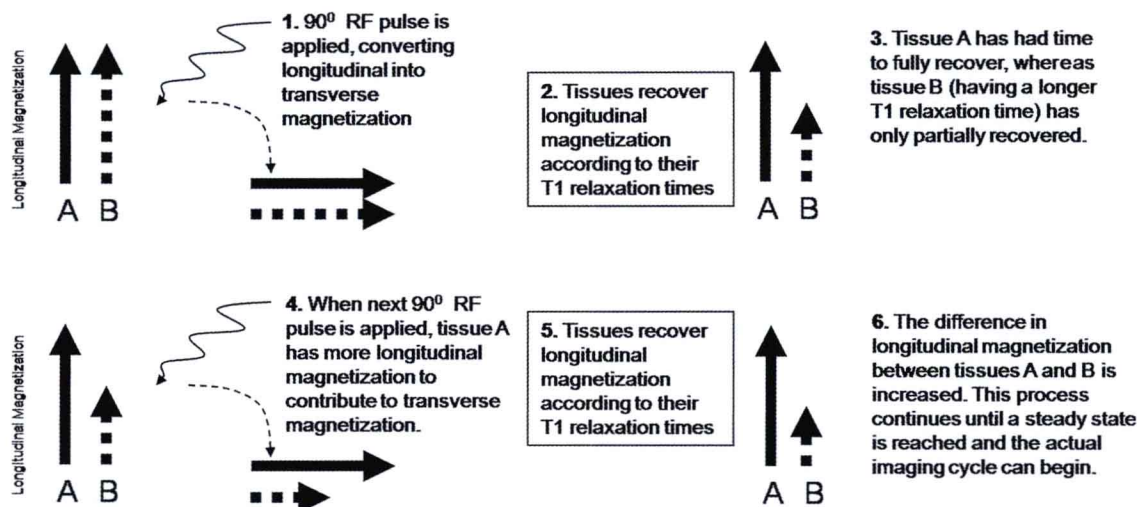


FIG. 1.1.8. Creation of equilibrium for longitudinal magnetization. Tissue A (solid line) has a short T1, whereas tissue B (dotted line) has a relatively long T1. After the initial application of the RF pulse, longitudinal magnetization of both tissues is converted into transverse magnetization. The tissues then recover longitudinal magnetization at different rates according to their respective T1 values. Because tissue B is not fully recovered between successive RF pulses, it loses longitudinal magnetization relative to tissue A. In this manner, an equilibrium (or steady state) is created for the longitudinal magnetization of the two tissues. When the actual imaging cycle is initiated, tissue B will have less longitudinal magnetization to convert into transverse magnetization. Less transverse magnetization for tissue B results in lower signal intensity for tissue B on the final image.

gradient reversal (in the case of gradient echo) must be repeated many times. Each time this series of events is repeated, a different strength gradient (referred to as the **phase-encoding gradient**) is applied to impart a phase difference upon the protons of interest. The TR is the time between one excitation pulse and the next. In other words, for a standard spin echo sequence, the TR is the time interval between successive 90-degree pulses. In general, a long TR allows for full recovery of longitudinal magnetization within tissues, regardless of their respective T1 values. Therefore, tissues cannot be differentiated on the basis of their T1 values when a long TR (relative to the tissue T1 values) is used. On the other hand, a short TR allows only enough time for tissues with a short T1 to recover a significant amount of longitudinal magnetization. Therefore, a short TR allows for differentiation of tissues on the basis of their respective T1 values. In reality, before collecting any echoes, a state of equilibrium is established in the tissue through the application of repeated RF pulses at the TR specified (Fig. 1.1.8). The number of preparatory pulses needed to reach equilibrium varies with pulse sequence, TR, and flip angle.

The time from the center of the excitation pulse to the center of the echo is known as “TE.” The refocusing pulse occurs halfway between the excitation pulse and the echo (at TE/2). A long TE allows more time for signal loss to occur from T2 decay. Therefore, a long TE allows for substantially greater signal loss from tissues with a short T2 than from tissues with a long T2 (Fig. 1.1.9). In other words, a long TE allows for differentiation of tissues on the basis of their respective T2 values. Another important point is that a long TE allows more time for the effects of

local magnetic field heterogeneities (T2* effects) to occur. As a result, magnetic susceptibility artifacts resulting from metal or air are exaggerated with most MR sequences when imaging is performed with a longer TE (Fig. 1.1.10).

k-SPACE

The concept of **k-space** has confounded radiology trainees since MRI was first developed. Most of the confusion stems from its name, which provides no hint to the clinically inclined as to its meaning.* In fact, k-space is not a space at all. It can be thought of as a digital representation or matrix of the multiple echoes produced during MRI. It is a map of the spatial frequency components that make up an image.

To better understand k-space, it helps to think of an image as a spectrum of spatial frequencies or collection of sine waves of varying amplitude, phase, and frequency that, when combined, create a picture. This is somewhat analogous to a symphony consisting of sound waves of different volumes and pitches. Each data point in k-space is *not* representative of a particular pixel in the final image. Rather, each k-space data point describes a sinusoidal waveform that contributes to the entire image. The more complete the data in k-space, the more closely the

*The “k” in k-space refers to a mathematical term used by convention to define spatial frequency. This term appears in the mathematical description of the MR signal and has, unfortunately, become entrenched in the MR lexicon.

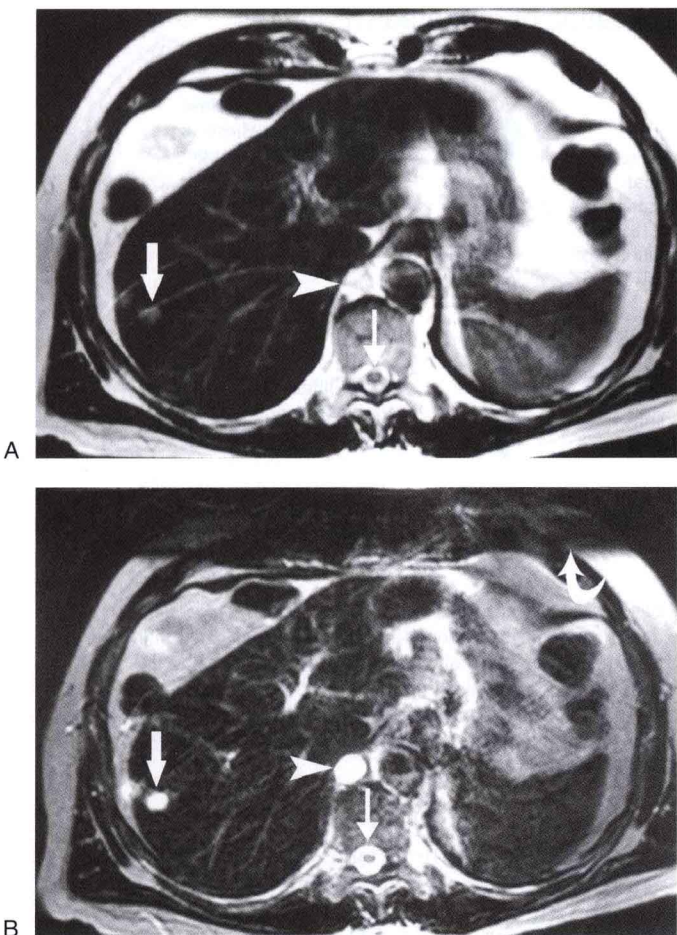


FIG. 1.1.9. Effect of TE on T2W image. A: TE = 100 msec. Small hemangioma (arrow), cerebrospinal fluid (CSF) (thin arrow), and cisterna chyli (arrowhead) are not significantly different in signal intensity from fat. B: TE = 250 msec. Small hemangioma (arrow), CSF (thin arrow), and cisterna chyli (arrowhead) are significantly more conspicuous due to loss of signal intensity of background tissues having shorter T2. Note the use of a saturation band (curved arrow) over anterior subcutaneous fat to decrease respiratory artifact on this non-breath-hold examination.

final image will resemble the source of the signal (in this case, the body).

One might wonder how the data in k-space come about. When a population of spinning protons is flipped into the transverse plane, it has a net transverse magnetization vector that rotates in the transverse plane. When refocused, this rotating vector (a time-varying magnetic field) induces a current in the receiver coil. This analog signal, or echo, consists of contributions from all the voxels in the image slice. However, through the application of the frequency and phase-encoding gradients, this echo is made to fill a specific line of k-space with data. Before the line of k-space can be filled, the analog signal must be converted to digital data by sampling it periodically during application of the “**readout**” gradient (also referred to as the **frequency-encoding gradient**).

Many echoes are collected to make an image—one for each application of the **phase-encoding gradient**. Each time an echo is produced, the echo is sampled multiple times during application of the readout gradient and

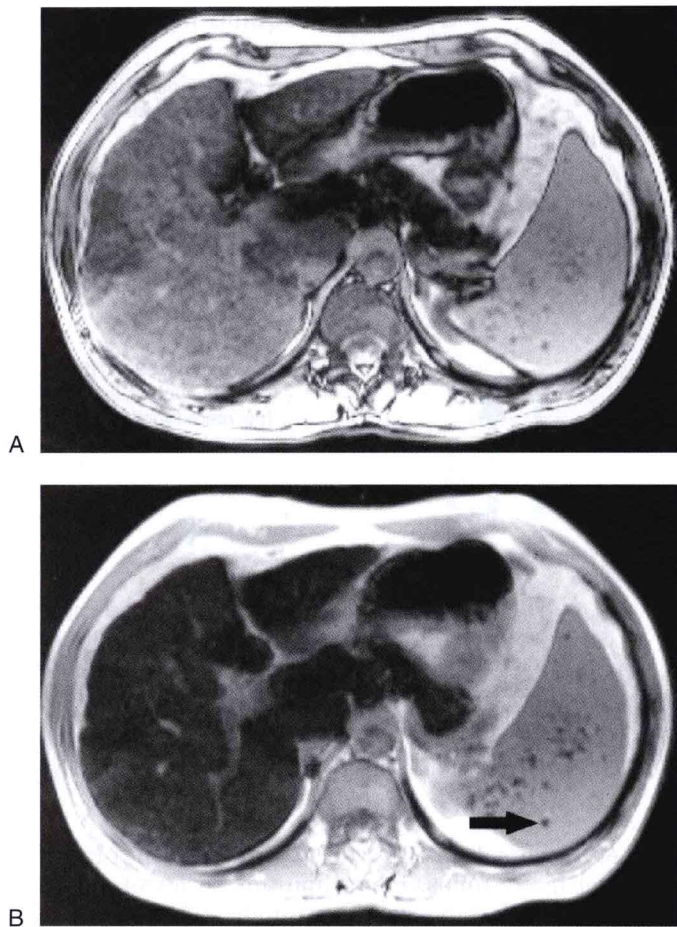


FIG. 1.1.10. Effect of increasing echo time (TE) in a patient with hemochromatosis. A: Gradient echo T1W image with TE = 2.7 msec. B: Gradient echo T1W image in the same patient with TE = 5.3 msec. Note the lower signal intensity of liver relative to spleen with longer TE due to greater dephasing induced by the presence of parenchymal iron. Siderotic nodules within spleen (arrow) are also more conspicuous.

converted into digital data through the use of an analog-to-digital converter. The rate of data sampling is determined by the **receiver bandwidth**. In a traditional k-space trajectory, each echo fills one line of k-space. If a spatial resolution of 256 image lines is desired in the phase-encoding direction, 256 phase-encoding steps must be completed, although there are ways of getting around this requirement, which will be discussed in the next chapter.

Once all of the echoes are digitized and k-space is filled to the desired extent, a form of **Fourier transformation** of the digital data is used to create an image (Fig. 1.1.11). A Fourier transform describes the deconstruction of a signal into its component frequencies and phases. Strictly speaking, the creation of an MR image from its spatial frequency components involves an inverse Fourier transform, but knowing that will not make the PACS worklist any shorter. All of these formidable calculations account for some of the delay between data acquisition and image display.

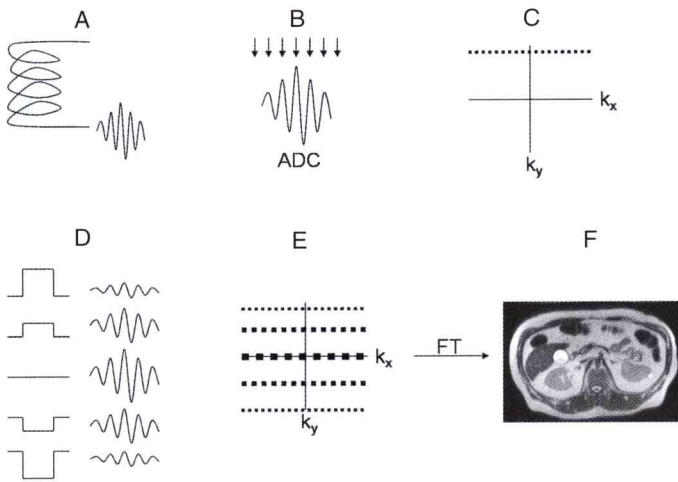


FIG. 1.1.11. From echoes to MR image. This figure picks up where Figure 1.1.5 left off. **A:** An analog signal (the echo) is detected with the receiver coil. **B:** The echo is sampled during application of the readout gradient to convert it to digital form by the analog-to-digital converter (ADC). The sampling rate is controlled by the receiver bandwidth. **C:** The digital data are used to fill a line of k-space (this illustrates a Cartesian trajectory). **D:** For a typical magnetic resonance (MR) image acquisition, multiple echoes are collected. Each echo is created using a different amplitude of the phase-encoding gradient. **E:** Each echo is digitized and fills a line in k-space. **F:** A type of Fourier transform (FT) is performed to convert the data in k-space into an image.

Several properties of k-space are salient to the clinical practice of MRI. Data points close to the **center of k-space** (i.e., those obtained during the application of weak phase-encoding gradients and when maximum rephasing has occurred) have the highest amplitude and contribute most to image contrast. These points also correspond to low spatial frequencies. Data points near the **periphery of k-space** (i.e., those obtained during application of strong phase-encoding gradients and when the protons have only partially rephased) contribute most to spatial resolution and edge definition, as these correspond to high spatial frequencies. An image can be made from only a portion of k-space; however, such an image may lack image contrast, spatial detail, or both. For most MR applications, the central lines of k-space are the most critical, particularly for high-contrast techniques such as MR angiography (MRA).

The relative position of the data points in k-space also controls image resolution and field-of-view. The overall size of k-space determines the image resolution, whereas the spacing between data points in k-space determines the field-of-view. Increasing the overall size of k-space by adding data points, while maintaining the same spacing between data points, improves spatial resolution without changing the field-of-view. Increasing the size of k-space by increasing the interval between the same number of data points improves resolution while decreasing field-of-view. Increasing the number of data points without increasing the overall size of k-space (by adding additional data points between the preexisting ones) increases the field-of-view without changing image resolution. Decreasing the interval between data points without adding additional ones contracts k-space, resulting in a

larger field-of-view at the expense of decreased resolution. Figure 1.1.12 illustrates various manipulations of data in a simplified version of k-space and the subsequent effects on the resulting images.



GRADIENTS

Producing a signal or echo is only the first step in creating an MR image. Equally important is localizing the signal in space. This may seem an impossible task, because the echo measured in MRI represents signal from the entire volume of tissue excited by the initial RF pulse, and this signal appears graphically like a wavy line. However, the data can be spatially encoded through the use of gradients, and the spatial information contained in the signal can be extracted by applying a variation of Fourier transformation. As mentioned earlier, a **gradient** is a linear variation in the magnetic field strength along an axis (although the term “gradient” is also used to refer to the gradient coils that produce this variation in magnetic field strength). Because the MR signal must be localized in three dimensions (3D), spatial encoding requires the use of three gradients.

The **slice-select gradient** is the easiest to understand. To produce signal from only one slice during a 2D acquisition, a gradient is applied along an axis perpendicular to the desired slice. Because the magnetic field strength varies along this axis, the hydrogen protons precess at different rates on the basis of their location relative to this gradient according to the Larmor equation. A frequency-selective RF pulse (i.e., an RF pulse of a specific frequency) excites only those protons precessing at the same frequency as the transmitted RF pulse. Therefore, protons at only a specific location along the gradient are tipped into the transverse plane and contribute to the final echo. The location of the tissue (slice) to be excited is controlled by the **center frequency**. The range of frequencies transmitted during this process is referred to as the **transmit bandwidth**. While the center frequency controls the location of the imaging slice along the slice-select gradient direction, the slice thickness is controlled by the transmit bandwidth and the steepness of the gradient. Because slice profiles are not perfectly rectangular, but rather taper on either side, the RF pulse used to excite one slice can partially affect adjacent slices. This can result in a loss of image signal and contrast and create undesirable artifacts (commonly referred to as “cross talk”). For this reason, a small gap is often inserted between slices of a sequential 2D acquisition.

As noted, three gradients are required to create an image of a 3D structure, even if only one slice is acquired. The other two gradients are the **frequency-encoding gradient** and the **phase-encoding gradient**. To create an image that is anatomically (spatially) accurate, each line of k-space must be filled with data. The order in which the lines are filled is determined by the amplitude and duration of the frequency- and phase-encoding gradients.

The frequency-encoding gradient spatially localizes protons along an axis perpendicular to the slice-select gradient (i.e., in the plane of the slice) by causing the protons along this gradient to resonate at different frequencies